www.czasopisma.pan.pl PAN POLSKA AKADEMIA NAUK www.journals.pan.pl

Arch. Metall. Mater. **67** (2022), 4, 1251-1257

DOI: https://doi.org/10.24425/amm.2022.141049

R.G. CHELARIU[1], N. CIMPOEȘU[1*], T.I. BIRNOVEANU[1], B. ISTRATE[2], C. BACIU[1], C. BEJINARIU[1]

OBTAINING AND ANALYSIS OF A NEW ALUMINIUM BRONZE MATERIAL USING INDUCTION FURNACE

Copper-based alloys with the addition of Al present excellent properties and can be considered a proper choice for applications as contact materials based on their good strength and fret resistance. Cu-Al alloys are used in different systems parts as bearings, gears and worm gears. The intention is to replace steel materials with new copper-based materials for parts that work in a possible explosive environment to reduce the possibility of spark appearance. Copper-berilyum alloys are known as non-sparking alloys and are used in different tools obtaining for environments with possible explosive gaseous. Results from the obtaining and analysis of a new alloy based on CuAlBe are given. The material was melted in a vacuum induction furnace from CuBe master alloy and high purity aluminium and cast into a metallic die. The alloys obtained were analyzed using EDS – energy dispersive spectroscopy for chemical composition, OM-optical and SEM-electronic microscopy for the microstructure, and the electro-corrosion resistance was tested using linear Tafel diagram and cyclic potentiometry.

Keywords: Aluminum bronze; non-sparking alloy; SEM; EDS; Tafel

1. Introduction

Aluminum bronzes are the most widespread and most valuable special bronzes due to their superior properties. Aluminum bronzes can be binary (simple) alloys, when copper is alloyed only with aluminum, or complex bronzes, when in addition to aluminum, they also contain other alloying elements such as iron, manganese, or nickel [1]. The alloys with 7%-10% Al, will have a structure formed by solid solution β up to a temperature of approx. 850°C when phase α begins to separate, and phase β will decompose after a eutectoid transformation. Due to the presence of the eutectoid ($\alpha + \gamma_2$), the alloy acquires superior mechanical characteristics in terms of strength and hardness. The addition of various elements in aluminum bronzes brings an improvement in their properties. Iron determines the finish of the structure, increases the tensile strength and hardness but decreases fluidity [2-4].

Considered special bronzes, Cu-Al alloys represent the most valuable group due to their high mechanical and technological characteristics, being able to successfully replace various metallic materials. In terms of oxidation and corrosion resistance, aluminum bronzes are among the best copper-based alloys, successfully replacing even stainless steels [5-7]. These alloys are well corrosion-resistant caused by mineral and organic acids, fresh or salt water and atmospheres of hydrogen sulfide and sulfur dioxide, in chloride and chlorate solutions, because of surface passivation due to the formation of Al_2O_3 film, which resists the action of reducing substances. The mechanical properties are superior to other copper alloys and even to Fe-C alloys, and depend on both the structure and addition of other elements in the chemical composition [8].

The mechanical tensile strength is directly proportional to the amount of eutectoid ($\alpha + \gamma_2$). If the structure of aluminum bronzes consists of α phase (up to 5-6% Al), the mechanical strength has modest values (20-25 daN/mm^2); it registers an important jump (up to 50-60 daN/mm^2) if the structure consists of phases $\beta + (\alpha + \gamma_2) + \alpha$ (9-11% Al). As the Al content increases (over 12%), the mechanical strength decreases due to the increase in the proportion of hard and brittle β phase. The hardness of these alloys increases as the β-phase content in the structure increases, reaching maximum values of 350-400 HB. The elongation of bronzes with aluminum increases proportionally with the α phase content, reaching maximum values (of about 30%) for alloys with β + α structure [9,10].

In this article the authors recommend a new solution for materials that are used in possible explosive environments

[1] "GHEORGHE ASACHI" UNIVERSITY OF IASI, FACULTY OF MATERIALS SCIENCE ENGINEERING, PROF.DR.DOC. D. MANGERON STREET, NO. 41, IAȘI 700050, ROMANIA
[2] "GHEORGHE ASACHI" UNIVERSITY OF IASI, FACULTY OF MECHANICAL ENGINEERING, PROF.DR.DOC. D. MANGERON STREET, NO. 61-63, IAȘI 700050, ROMANIA

* Corrersponding author: nicanor.cimpoesu@tuiasi.ro

© 2022. The Author(s). This is an open-access article distributed under the terms of the Creative Commons Attribution-NonCommercial License (CC BY-NC 4.0, https://creativecommons.org/licenses/by-nc/4.0/deed.en which permits the use, redistribution of the material in any medium or format, transforming and building upon the material, provided that the article is properly cited, the use is noncommercial, and no modifications or adaptations are made.

(natural gaseous, petroleum systems or pipes, gears etc.) where a certain mechanical resistance is required and can be provided by metallic materials. Although new non-spark materials are investigated, like CuNiSn, to replace the alloys with beryllium for certain environmental applications, the Cu-Al-Be present better mechanical properties necessary for gear applications and remains the best solution as non-spark material.

2. Experimental set-up

To obtain one or another of the brands of aluminum bronzes, the smelting process can be started either from pure metal elements or from various kinds of aluminum bronzes in the form of ingots or waste. The metal load in the case of aluminum bronzes can be composed of the following: cathode copper, (various brands); technical aluminum, SREN 576 – 2004 and SREN 1676 – 1998; technical aluminum waste from electrical or other fields: bars, wires, sheets, etc; Cu-Al pre-alloy ingots. The elaboration of bronzes with aluminum from elements supposes the completion of the following operations: a) cleaning of the elaboration furnace; b) heating the processing furnace until its refractory lining has reached a temperature of 800-900°C (bright red); c) on the bottom of the furnace hearth or on the bottom of the crucible will be loaded a quantity of coating fondant appreciated as sufficient to cover the surface of the metal bath to be formed; d) place the cathode copper or copper scrap pieces in the oven; e) fill the load with smaller pieces of metal material not initially introduced;f) continue melting until the temperature of the metal bath reaches 1150-1200°C, following the completion of the protective flow layer; g) stop the oven and pour the deoxidation sample; h) depending on the configuration of the sample, the elaboration course is decided; i) allow the bath to settle and cool to a temperature of 1120-1140°C in order to introduce the aluminum. j) insert metallic or pre-alloy aluminum, preheated to 150-180°C, in the metal bath under the slag layer; k) homogenize the bath with a steel bar, so as not to "break" the slag layer or it is entrained in the melt; l) the other alloying elements will be introduced in the form of pre-alloy or in solid state: proceeding to the homogenization of the bath; m) the melt is overheated to the casting temperature, chosen according to the parts to be poured, and it will be maintained at this temperature approx. 5-10 min. n) turn off the oven and remove the slag; o) the bronze is evacuated in the preheated red casting pot; p) pour in as short a time as possible, from as low a height as possible.

A part of the charge was taken separated for laboratory experiments. The experiments were performed in accordance with the occupational health and safety laws and regulations to eliminate all risks and dangers that can affect the human resource during the experiment procedures [11-13].

NDT test was made after the melting of alloys using fluorescent penetrant liquids. Chemical composition was determined after casting the experimental alloys and after the electro-corrosion test with an EDS detector from Bruker X-Flash in element list mode. The microstructure was determined after mechanical grinding of the materials until 2000 grid with SiC papers, polished with alumina solution and chemical etching with $FeCl_3$ for 2-5 seconds. Optical micrographs were realized on the structure using a Zeiss metallographic microscope with Motic specialized acquisition camera and software [14]. A VoltaLab 21 Electrochemical System (PGP201-Economical Potentiostat) was used for the corrosion analysis, equipped with a VoltaMaster 4 data acquisition and processing software. The corrosion analysis system consists of an electrochemical cell with three electrodes, one saturated calomel as the reference electrode, a platinum electrode used as auxiliary electrode and a working electrode.

The sample subjected to the electro-corrosion process was cleaned and washed with distilled water before the experiment. 0.9% NaCl electrolit solution was used at room temperature. The linear polarization curves were plotted with the scanning speed of the electrode potential dV/dt = 0.5 mV / s, and the cyclic polarization curves with a speed of 10 mV/s.

The surface after electro-corrosion tests was analyzed using scanning electron microscopy (SEM-FEI model Quanta200).

3. Experimental results

The experimental alloys were washed in the ultrasonic chamber before the NDT analysis. This test is hydrophilic post emulsification. To this end, we used an ultra-high sensitivity level 4 penetrant solution and a hydrophilic emulsifier in 5% concentration. A dry developer was used for a better contrast, that amplifies the location of pores. Steps used for each stage were as follows: penetrant dwell time 20 min, emulsifier time 2 min and developer time 10 min. The parts were inspected under UV light with an intensity of 3800 $\mu W/cm^2$ measured at 38 cm distance from the lamp's bulb [15]. After the melting/casting stage the materials were analyzed, on the surface, with fluorescent penetrant liquids to observe if voids, cracks or holes appear on the alloy. In Fig. 1 can be observed a clean surface for all three experimental alloys meaning that a homogeneous material was obtained.

Through chemical composition analyze elements copper, aluminum and berilium were qualitatively identified in the energy spectrum from Fig. 2. A general analysis of the chemical element's distribution, Fig. 2, presents a chemically homogeneous material without specific agglomerations or area depleted in some of the chemical elements.

The quantitative chemical analysis, in weight and atomic percentages %, TABLE 1, present the differences obtained in the chemical composition of, from now on called, experimental alloys: Alloy 1, Alloy 2 and Alloy 3. The first two alloys considered for analysis have appropriate percentages of Cu and Be with differences between Al and alloys 2 compared to 3 has appropriate Al and Cu percentages and different mass percentage of Be. In this article, we follow the influence of addition elements (Al and Be) to the Cu matrix to electro-corrosion resistance.

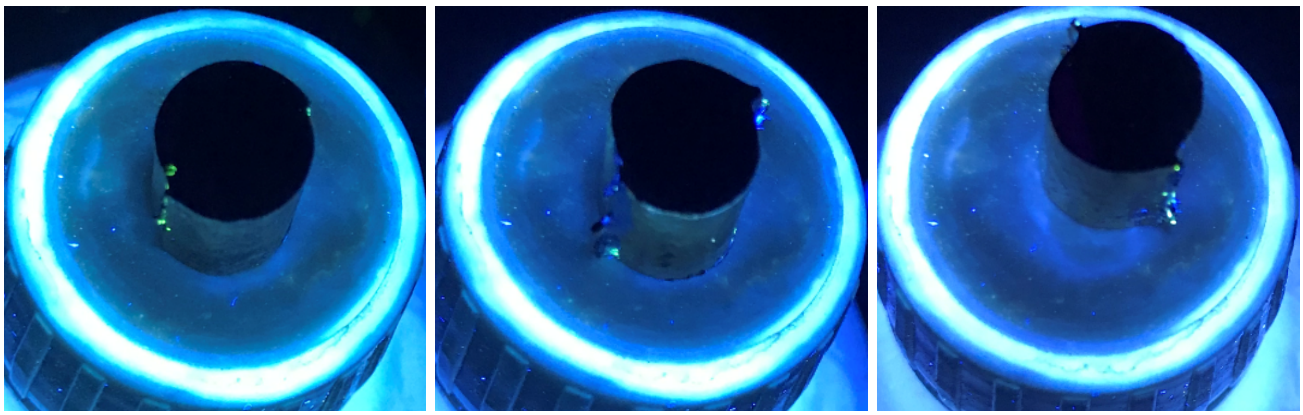

a) b) c)

Fig. 1. NDT results a) alloy 1, b) alloy 2 and c) alloy 3 after five re-melting operations

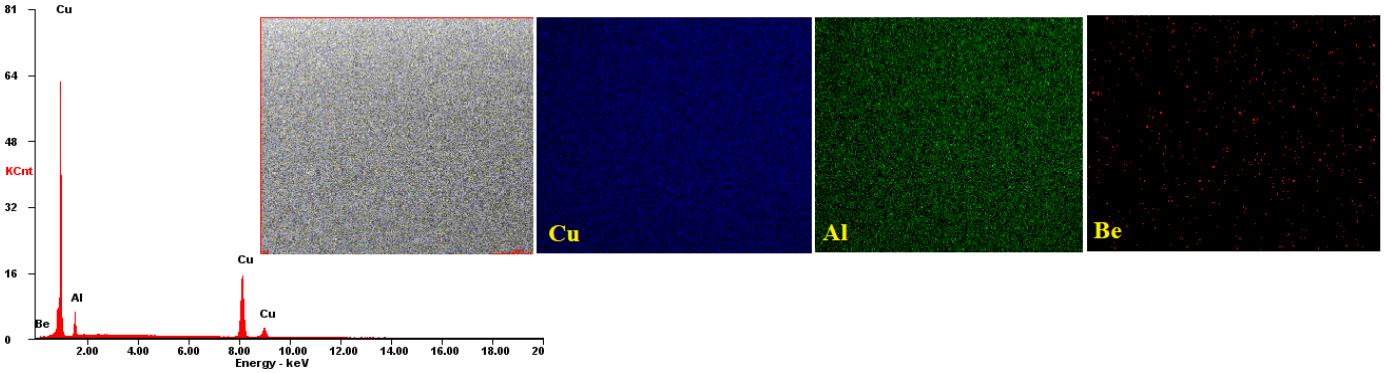

Fig. 2. Chemical composition determination, energy spectrum and main elements distribution

TABLE 1

Chemical composition from 5 areas of the experimental materials

Chemical elements	Alloy 1		Alloy 2		Alloy 3	
	wt%	at%	wt%	at%	wt%	at%
Cu	90,71	78,0	89,12	76,21	84,47	58,06
Al	8,5	17,22	10,41	20,97	10,32	16,7
Be	0,79	4,78	0,47	2,82	5,21	25,24

The microstructure of the alloys, Fig. 3, highlighted by optical microscopy, presents a big grain structure for all cases. The grains are big of hundreds of micrometers in all cases. The grain baunderies seems thick and present precipitates. In the first alloy case, Fig. 3a), in grain martensitic type plates can be observed. Especially in fist alloy case and partially in third we can observe a homogeneous spread of precipitates of $CuAl_2$. Coarse compounds are situated at the grain boundaries and at the common limits of the grains, places representing the easiest places for nucleation. The smaller grain presents a finer structural relief. The areas appropriate to the boundaries with precipitates show a lack of compounds mainly on Cu-Al matrix [16-20].

The differences in the chemical composition based on the presence of precipitates between the grain limits and the grains will be an important and predominant factor in electro-corrosion resistance of the alloys when the potential difference between

a) b) c)

Fig. 3. Optical micrographs of the alloys structure (chemical etch $FeCl_3$) a) alloy 1, b) alloy 2 and c) alloy 3

these two areas will create electro micro-piles in the salt electrolyte solution. On the structure of the third alloy, Fig. 3c), the spread of precipitation is more homogeneous, not only at grain boundaries but also inside the grains.

4. Electro-corrosion resistance of experimental materials

Copper and its alloys are recognized as materials with good corrosion resistance and are thus used in many fields of activity [21,22]. The good resistance of these materials is related to the formation on the surface of a uniform and adherent film (oxides, hydroxides, etc.) that protects the substrate from the environment. When corrosion occurs in aqueous medium, copper anodically dissolves with the formation of ions [23]: Cu^{2+} and Cu^{+}:

$$Cu = Cu^{+} + e^{-}$$

$$Cu^{+} = Cu^{2+} + e^{-}$$

In the presence of HO^{-} and Cl^{-} ions, and depending on the pH of the solution, Cu^{+} and Cu^{2+} ions can lead to insoluble products (Cu_2O, CuO, Cu (OH), $Cu(OH)_2$) capable of forming protective barriers, under film form, by reactions such as:

$$2Cu^{+} + 2HO^{-} = Cu_2O + 1/2\ H_2O$$

$$Cu^{+} + Cl^{-} = Cu_2O + 2H^{+}$$

$$Cu_2O + 2HO^{-} + H_2O = Cu(OH)_2$$

$$CuCl + H_2O = Cu_2O + 2H^{+} + 2Cl^{-}$$

$$2Cu^{+} + H_2O = Cu_2O + 2H^{+}$$

$$CuCl + 2HO^{-} = Cu_2O + H_2O + 2Cl^{-}$$

$$Cu_2O + 2HO^{-} = 2CuO + H_2O + 2e^{-}$$

The appearance of corrosion phenomenon is related to the formation and stability of this film; if the film is not formed or destroyed, the metal is corroded, either generalized – on the entire surface, or localized (cracks, fissures, pitting corrosion).

The polarization resistance method was used to evaluate the corrosion rate. This method is used to determine the corrosion current at the corrosion potential of the metal or alloy, from the linear polarization curve obtained for relatively small overvoltage. The corrosion current determined using this method therefore represents the current that appears at the metal/corrosive environment interface when the metal is immersed in the solution and represents the instantaneous corrosion current. In Fig. 4a) Tafel interpretation of linear potentiometry is presented and in Fig. 4b) the cyclic polarization curves are plotted.

The density of the corrosion current was calculated using the relation [24]:

$$J_{corr} = \frac{b_a \cdot b_c}{2.303(b_a + b_c) \cdot R_p}\ (\mathrm{mA/cm^2}) \qquad (1)$$

For the evaluation of the instantaneous corrosion current, the linear polarization curves recorded at the low potential rate (0.5 mV/s), obtained over the potential range (E_{cor} ± 150 mV) were used. The results obtained for the three alloys are presented in TABLE 2.

TABLE 2

Electro-corrosion resistance test parameters

Alloy	OCP mV	E_0 mV	b_a mV	b_c mV	R_p kohm.cm²	J_{corr} µA/cm²	V_{corr} µm/Year
1	–340	–342.9	168.5	–337.8	1.25	26.07	365.0
2	–304	–298.8	117.7	256.2	0.954	28.77	402.9
3	–230	–260.8	112.1	103.5	1.45	10.83	151.6

Based on the data presented in table 2, the following conclusions can be highlighted: all three alloys have open circuit potential, respectively, corrosion potential, negative values, which highlights the fact that, from a thermodynamic perspective, the natural tendency of these alloys is spontaneous corrosion. It is observed that increasing the percentage of Al [25,26], in the case of Alloy 2 up to 10%, does not significantly influence the corrosion resistance. Instead, increasing the percentage of Be, up to 5%, in the case of Alloy 3 decreases the corrosion current density from 28.77 to 10.83 µA/cm².

The analysis of the cyclic corrosion diagram, Fig. 4b), shows the general character of corrosion. There are no variations in the current density with potential. There were short periods of

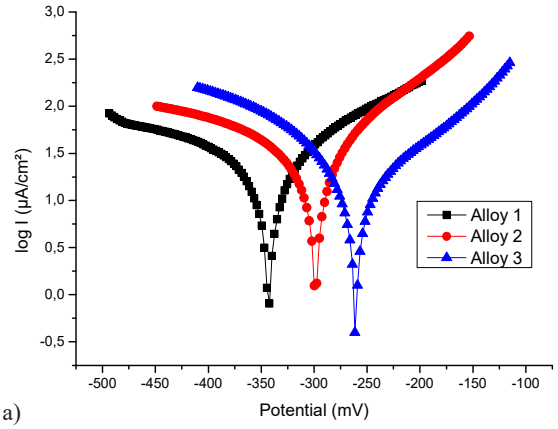

a)

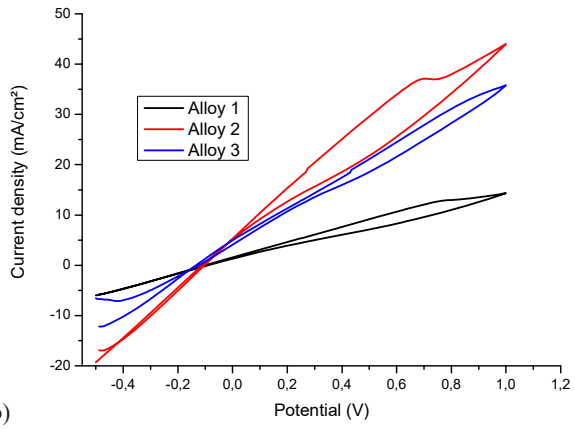

b)

Fig. 4. Electrochemical variations a) Tafel and b) cyclic voltamograms

passivation after the formation of Cu oxides. Third alloy present the smaller corrosion rate per year less than half comparison to the first alloy. This alloy presents the highest Be percentage and around ten percentages of aluminum.

After eletro-corrosion tests in salt electrolyte solution, a reddish layer was observed on the surface of the alloys. Chemical composition determination identifies beside based elements: Cu, Al and Be also few new elements from the salt electrolyte solution, especially oxides – red and salts like NaCl that passes from the solution to the alloy surface during the electro-corrosion tests, their qualitative presence was determined through EDS analyze and observed in the energy spectrum from Fig. 5a). In all cases, the surface was covered with a red oxide, copper oxide, with different morphologies, Fig. 5b)-d).

In the first alloy case the layer that covers the surface follows the grains positioning with differences in the boundaries. For the other two alloys, 2 respectively 3, the layer is formed from many small oxides with round and rectangular shapes.

In TABLE 3 the average values of the chemical composition of the alloy surface after five determinations in different areas. The oxygen, chlorine and natrium presence was observed after the electro-corosion test. Normally a composed oxide layer form on top of the surface based on CuO and Al_2O_3 that will protect the alloy from further and continuous corrosion [27,28]. Be element

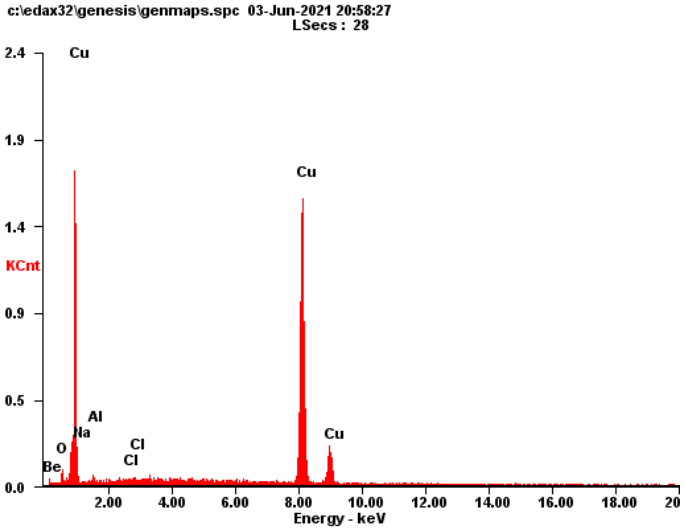

a)

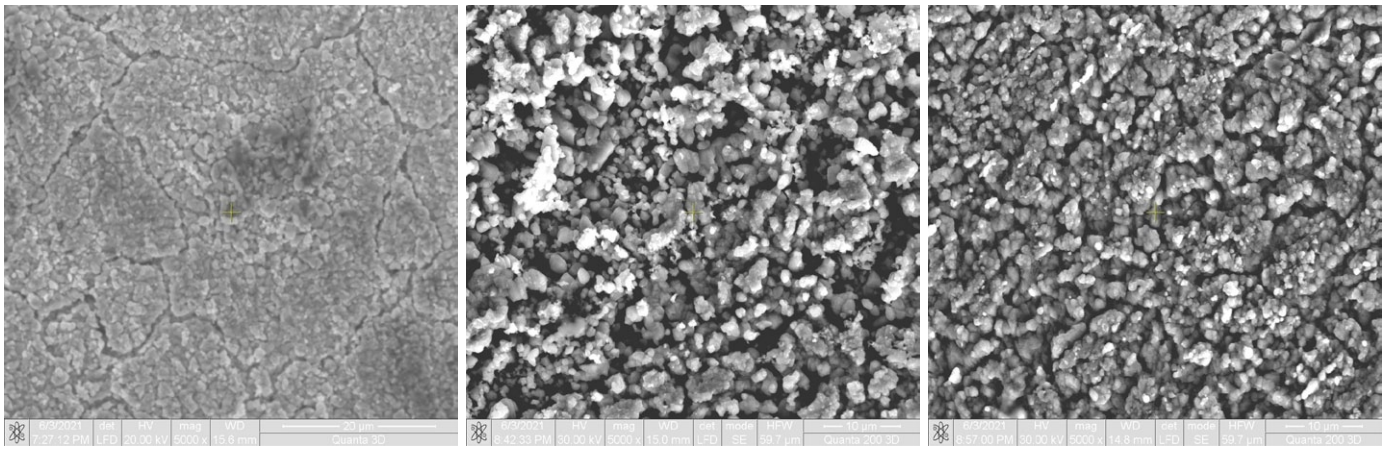

b) c) d)

Fig. 5. Surface statement of the alloys after electro-chemical corrosion test a) energy spectrum b) alloy 1, c) alloy 2 and d) alloy 3

TABLE 3

Chemical composition of the alloys surface after the electro-corrosion test (average of the results from five different areas)

Alloy	Cu		Al		Be		O		Cl		Na	
	wt%	at%	wt%	at%	wt%	at%	wt%	at%	wt%	at%	wt%	at%
Alloy 1	92.96	73.59	1.62	3.03	2.86	15.98	2.15	6.75	0.31	0.43	0.1	0.23
Alloy 2	91.22	66.24	1.05	1.8	4.91	25.16	1.72	4.97	0.51	0.67	0.58	1.17
Alloy 3	85.29	52.65	1.71	2.49	7.72	33.59	3.32	8.13	0.33	0.37	1.63	2.79
EDS error	0.9		0.2		0.1		0.25		0.1		0.1	

appears in a higher percentage than in the initial state based on the oxidation of the other two elements Cu and Al. The copper oxidases further in the third alloy case [29,30].

Part of the chlorine is from NaCl salt that passes from the salt solution to surface the other part from Cl ions that interact with the metallic material. Compared with the initial state a much smaller percentage of aluminium is observed in all cases. Most of the aluminum from the alloy interacts with oxygen forming alumina type layer and is most of him under or combined with the copper oxide.

5. Conclusions

Few conclusions can be structured from the research results:

– a new copper-based material alloyed with Al and Be was obtained through the classical induction furnace.
– three alloys with different chemical compositions were obtained through CuBe master alloy adding in an induction furnace (). Phosforescent penetrant liquids (NDT) present a homogeneous matrix formed after melting without voids, microcracks or micropores. The microstructure presents a structure with big grains, few hundreds of micrometers, with precipitates $CuAl_3$ at the grain limits and a depletion of precipitates near the boundaries inside the grains. The distribution of precipitates influences the electro-corrosion resistance of the alloy by creating electro-corrosion micro-piles. The differences in the corrosion rate can also be attributed to the chemical differences between the alloys (higher Be wt% content for a smaller corrosion per year).

REFERENCES

[1] X. Liu. D. Huang. C. Yan. Y. Zhou. W. Yan. Multi-directional forging and aging treatment effects on friction and wear characterization of aluminium-bronze alloy, Mater. Charact. **167**, 110511 (2020).

[2] M. Ienciu, P. Moldovan, N. Panait, M. Buzatu, Development and casting of non-ferrous alloys, EDP, Bucureşti, (1982).

[3] L. Wen-sheng, W. Zhi-ping, L. Yang, G. Yong, X. Jian-lin, Preparation, mechanical properties and wear behaviours of novel aluminium bronze for dies, Trans. Nonferrous Met. Soc. China **16**, 607-612 (2006).

[4] Z. Han, Y.F. He, H.C. Lin, H. Zhao, Dealloying characterizations of Cu-Al alloy in marine environment, J. Mater. Sci. Lett. **19**, 393-395 (2000).

[5] H.J. Meigh, Rought aluminium bronzes properties, processes and structure, Maney Publishing, ISBN 978-1-906540-20-3 (2008).

[6] M. Makeshkumar, S.R. Surender, S. Arunprakash, R. Madesh, M. Sasi Kumar, K. Sudharsan, Microstructural and mechanical properties evaluation of dissimilar aluminum alloy and bronze joints using friction stir welding, Materials Today: Proceeding (2021). DOI: https://doi.org/10.1016/j.matpr.2021.05.563

[7] Y. Li, Y. Lian, Y Sun, Comparison of cavitation erosion behaviors between the as-cast and friction stir processed Ni-Al bronze in distilled water and artificial seawater, J. Mater. Res. Technol. **13**, 906-918 (2021).

[8] N. Cimpoesu, S. Stanciu, D. Tesloianu, R. Cimpoesu, R. Popa, E. Moraru, A study of the damping capacity of mechanically processed Cu-9.2Al-5.3Mn-0.6Fe shape memory alloys, Met. Sci. Heat Treat. **58** (11-12), 729-733 (2017).
DOI: https://doi.org/10.1007/s11041-017-0086-0

[9] Y.-R. Su, T.-H. Wu, I.-C. Cheng, Synthesis and catalytical properties of hierarchical nanoporous copper from θ and η phases in CuAl alloys, J. Phys. Chem. Solids **151**, 109915 (2021).

[10] V.H.C. de Albuquerque, T.A. de A. Melo, R.M. Gomes, S.J.G. de Lima, J.M.R.S. Tavares, Grain size and temperature influence on the toughness of a CuAlBe shape memory alloy, Mater. Sci. Eng. A **528**, 459-466 (2010).

[11] C. Bejinariu, D.C. Darabont, E.R. Baciu, I. Ionita, M.-A. Bernevig-Sava, C. Baciu, Considerations on the Method for Self Assessment of Safety at Work. Environ. Eng. Manag. J. **16**, 1395-1400, (2017).

[12] D.-C. Darabont, R.I. Moraru, A.E. Antonov, C. Bejinariu, Managing new and emerging risks in the context of ISO 45001 standard, Qual.-Access Success **18**, 11-14 (2017).

[13] D.C. Darabont, A.E. Antonov, C. Bejinariu, Key elements on implementing an occupational health and safety management system using ISO 45001 standard. In 8th International Conference on Manufacturing Science and Education (MSE 2017) – Trends in New Industrial Revolution, Bondrea, I., Simion, C., Inta, M., Eds., E D P Sciences: Cedex A, 2017, Vol. 121, p. UNSP 11007.

[14] M.G. Zaharia, S. Stanciu, R. Cimpoesu, I. Ionita, N. Cimpoesu, Preliminary results on effect of H2S on P265GH commercial material for natural gases and petroleum transportation, Appl. Surf. Sci. **438**, 20-32 (2018).

[15] C. Panaghie, R. Cimpoesu, B. Istrate, N. Cimpoesu, M.-A. Bernevig, G. Zegan, A.-M. Roman, R. Chelariu, A. Sodor, New Zn3mg-xy alloys: Characteristics, microstructural evolution and corrosion behavior, Materials **14** (10), 2505 (2021).

[16] Z. Song, S. Kishimoto, J. Zhu, Y. Wang, Study of stabilization of CuAlBe alloy during martensitic transformation by internal friction, Solid State Commun. **139**, 235-239 (2006).

[17] V. Nedeff, C. Bejenariu, G. Lazar, M. Agop, Generalized lift force for complex fluid, Powder Technol. **235**, 685-695 (2013).
DOI: https://doi.org/10.1016/j.powtec.2012.11.027

[18] S. Montecinos, A. Cuniberti, Thermomechanical behavior of a CuAlBe shape memory alloy, J. Alloy. Compd. **457**, 332-336 (2008).

[19] S. Montecinos, S.N. Simison, Study of the corrosion products formed on a multiphase CuAlBe alloy in a sodium chloride solution by micro-Raman and in situ AFM measurements, Appl. Surf. Sci. **257**, 7732-7738 (2011).

[20] C.D. Florea, I. Carcea, R. Cimpoesu, S.L. Toma, I.G. Sandu, C. Bejinariu, Experimental Analysis of Resistance to Electrocorosion of a High Chromium Cast Iron with Applications in the Vehicle Industry, Rev. de chimie **68** (10), 2397-2401 (2017).

[21] T. Ma, B. Tan, L.G. Savas¸ K.Z. Kao, S. Zhang, R. Wang, N. Zeng, Y. He, Multidimensional insights into the corrosion inhibition of

potassium oleate on Cu in alkaline medium: A combined Experimental and theoretical investigation, Mat. Sci. Eng. B **272**, 115330 (2021).

[22] C. Zeng, B. Zhan, A.H. Ettefagh, H. Wen, H. Yao, W.J. Meng, S. Guo, Mechanical, thermal, and corrosion properties of Cu-10Sn alloy prepared by laser-powder-bed-fusion additive manufacturing, Additive Manufacturing **35**, 101411 (2020).

[23] G. Kear, B.D. Barker, F.C. Walsh, Electrochemical corrosion of unalloyed copper in chloride media – a critical review, Corros. Sci. **46**, 109-135 (2004).

[24] R. Cimpoesu, P. Vizureanu, I. Stirbu, A. Sodor, G. Zegan, M. Prelipceanu, N. Cimpoesu, N. Ioanid, Corrosion-resistance analysis of ha layer deposited through electrophoresis on Ti4Al4Zr metallic substrate, Appl. Sci. **11** (91), 4198 (2021).

[25] S. Montecinosa, P. Klímek, M. Sláma, S. Suarez, S. Simison, Corrosion behavior of a β CuAlBe shape memory alloy containing stress induced martensite, Appl. Surf. Sci. **466**, 165-170 (2019).

[26] C.-P. Liu, S.-J. Chang, Y.-F. Liu, J. Su, Corrosion-induced degradation and its mechanism study of CueAl interface for Cu-wire bonding under HAST conditions, J. Alloy. Compd. **825**, 154046 (2020).

[27] H.H. Kuo, W.H. Wang, Y.F. Hsu, Microstructural characterization of precipitates in Cu-10 wt.%Al-0.8 wt.%Be shape-memory alloy, Mater. Sci. Eng. A **430**, 292-300 (2006).

[28] A.M. Alfantazi, T.M. Ahmed, D. Tromans, Corrosion behaviour of copper alloys in chloride media, Mater. Des. **30**, 2425-2430 (2009).

[29] M. Chmielová, J. Seidlerová, Z. Weiss, X-ray diffraction phase analysis of crystalline copper corrosion products after treatment in different chloride solutions, Corros. Sci. **45**, 883-889 (2003).

[30] M. Wang, Y. Zhang, M. Muhammed, Critical evaluation of thermodynamics of complex formation of metal ions in aqueous solutions. III. The system Cu(I.II)-Cl-e at 298.15 K, Hydrometallurgy **45**, 53-72 (1997).